Effect of substitution and the counterion on the structural and spectroscopic properties of Cu[II] complexes of methylated pyrazoles

Ian D. Giles, Jeffrey C. DePriest & Jeffrey R. Deschamps

[+] View supplementary material ↗

📅 Accepted author version posted online: 10 Aug 2015.
   Published online: 28 Aug 2015.

✎ Submit your article to this journal ↗

📊 Article views: 73

🔍 View related articles ↗

⊙ View Crossmark data ↗

Taylor & Francis
Taylor & Francis Group

Effect of substitution and the counterion on the structural and spectroscopic properties of Cu^{II} complexes of methylated pyrazoles

IAN D. GILES† ⓘ , JEFFREY C. DEPRIEST‡ and JEFFREY R. DESCHAMPS*† ⓘ

†Center for Bio/Molecular Science and Engineering, Naval Research Laboratory, Washington, DC, USA
‡Counter Weapons Mass Destruction, Defense Threat Reduction Agency, Fort Belvoir, VA, USA
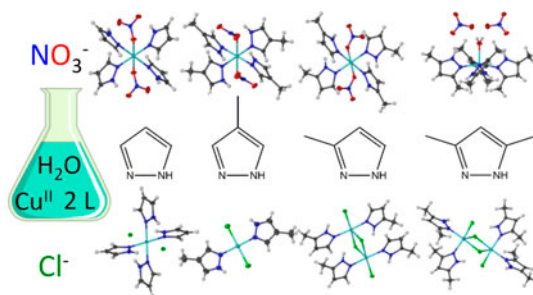
The coordination chemistry of pyrazole and three of its methyl derivatives with the chloride and nitrate salts of copper(II) under strictly controlled reaction conditions is systematically explored to gain a better understanding of the effect of counterion coordination strength and ligand identity on the structure and electronic absorption spectra of their resulting complexes. Despite the initial 2 : 1 ligand to metal ratio in water, copper(II) nitrate forms exclusively 4 : 1 ligand to metal complexes while copper(II) chloride forms a 4 : 1 ligand to metal complex only with pyrazole, with the methyl derivatives forming 2 : 1 ligand to metal complexes, as determined by single-crystal X-ray diffraction (XRD). This is attributed to a combination of ligand sterics and stronger coordination of chloride relative to nitrate. Electronic absorption spectroscopy in both water and methanol reveals a surprisingly strong effect of the pyrazole methyl position on the Cu^{II} d–d transition, with 4-methylpyrazole producing a higher energy d–d transition relative to the other ligands studied. In addition, the number of methyl groups plays a determining role in the energy of the pz π→Cu^{II} d$_{xy}$ LMCT band, lowering the transition energy as more methyl groups are added.

Keywords: Coordination chemistry; Pyrazole; Copper(II); Electronic spectroscopy; Single-crystal X-ray diffraction

---

*Corresponding author. Email: deschamps@nrl.navy.mil

1. Introduction

Pyrazoles have long been recognized as useful ligands for studying the coordination chemistry of first-row transition metals [1]. The current widespread availability of substituted pyrazole ligands makes them excellent synthons for a wide variety of applications. During the course of our studies involving pyrazole-based ligands, we wanted to explore the interplay between ligand substituent effects and anion coordination strength in the formation and crystallographic packing of their Cu^{II} coordination complexes in controlled reaction environments, as well as what effect changing the ligand substituent had on the electronics of the ligands and their complexes.

Specifically, our goal is reliably and predictably controlling ligand coordination (both number and mode) to Cu^{II} while maximizing the density of the compound in the crystal phase and tuning the complex's electronic properties. Although much work has been reported on Cu^{II} complexes of a wide variety of substituted pyrazole ligands, we were surprised to find that, while vibrational and electronic absorption data are widely reported, crystallographic data were harder to come by, especially for 3(5)-methyl- and 4-methylpyrazole. This is likely a result of the era in which many of the early complexes of pyrazole and its methylated congeners were first made, prior to the widespread use of single-crystal X-ray diffraction (XRD), in which analyzing the structural characteristics of these early coordination complexes relied primarily on vibrational and electronic absorption spectroscopies, elemental analysis, and EPR. Some more recent publications revisit these complexes and provide structural data for Cu^{II} complexes of pyrazole [2] and 3,5-dimethylpyrazole [3], but not 3(5)- or 4-methylpyrazole, and certainly not in any systematic manner.

Using consistent reaction and crystallization conditions, we have crystallized a series of eight Cu^{II} complexes incorporating pyrazole and its 3(5)-methyl, 4-methyl, and 3,5-dimethyl derivatives. The diversity of their respective single-crystal XRD structures lends insight into how the Cu^{II} coordination environment is affected by ligand substitution and the counterions of the initial Cu^{II} salt. Although the crystal structures determined for the Cu^{II} complexes of pyrazole and 3,5-dimethylpyrazole match established structures, they are presented again as obtained in the course of this study for direct comparison with the 3(5)- and 4-methylpyrazole complexes, whose crystal structures are presented here for the first time. The electronic absorption properties of these complexes are also revisited in an attempt to better understand the effects of pyrazole substituents on the electronic properties of Cu^{II}.

2. Experimental

All manipulations were carried out in air at room temperature with reagents as obtained from the manufacturer. $Cu(NO_3)_3 \cdot 2.5H_2O$ was purchased from Fisher Scientific while $CuCl_2 \cdot 2H_2O$ was purchased from Aldrich Chemical Company. Pyrazole and 4-methylpyrazole (fomepizole) were purchased from Aldrich, while 3,5-dimethylpyrazole and 3-methylpyrazole were purchased from Oakwood Chemical Company. Deionized water was used in all reactions. Crystals were obtained by slow evaporation of the reaction solution over the course of several days unless otherwise noted.

2.1. *Synthesis*

2.1.1. *trans*-[Cu(C$_3$H$_4$N$_2$)$_4$]Cl$_2$ (1). A light blue solution of 0.144 g (0.842 mmol) CuCl$_2$·2H$_2$O in 4 mL H$_2$O was added via pipette to a colorless pyrazole (0.114 g, 1.67 mmol) solution in 5 mL H$_2$O while stirring. A 1 mL rinse of the Cu^{II} vessel with H$_2$O was added to the reaction. An immediate reaction occurred, resulting in a color change to medium blue. The reaction was stirred overnight in capped vials, followed by crystallization via slow evaporation of H$_2$O to yield blue-purple single crystals. Yield: 0.165 g (97.1%). CCDC 1056654. Anal. Calcd for CuC$_{12}$H$_{16}$N$_8$Cl$_2$ + 0.075 CuCl$_2$ (%): C, 34.58; H, 3.87; N, 26.88; Cu, 16.39; Cl, 18.29. Found: C, 34.59; H, 3.49; N, 26.93; Cu, 16.14; Cl, 18.27.

2.1.2. *trans*-[Cu(NO$_3$)$_2$(C$_3$H$_4$N$_2$)$_4$] (2). A light blue solution of 0.180 g (0.773 mmol Cu (NO$_3$)$_2$·2.5 H$_2$O in 4 mL H$_2$O was added via pipette to a colorless pyrazole (0.104 g, 1.53 mmol) solution in 5 mL H$_2$O while stirring. A 1 mL rinse of the Cu^{II} vessel with H$_2$O was added to the reaction. An immediate reaction occurred, resulting in a color change to medium blue. The reaction was stirred overnight in capped vials, followed by crystallization via slow evaporation of H$_2$O to yield blue-purple single crystals. Yield: 0.168 g (95.3%). CCDC 1056653. Anal. Calcd for CuC$_{12}$H$_{16}$N$_{10}$O$_6$ (%): C, 31.34; H, 3.51; N, 20.87; Cu, 13.82. Found: C, 31.28; H, 3.51; N, 30.16; Cu, 14.07.

2.1.3. *trans*-[CuCl$_2${4-(CH$_3$)-(C$_3$H$_3$N$_2$)}$_2$] (3). A light blue solution of 0.144 g (0.85 mmol) CuCl$_2$·2H$_2$O in 4 mL H$_2$O was added via pipette to a colorless 4-methylpyrazole (0.136 g, 1.66 mmol) solution in 5 mL H$_2$O while stirring. A 1 mL rinse of the Cu^{II} vessel with H$_2$O was added to the reaction. An immediate reaction occurred, resulting in a color change to dark royal blue. The reaction was stirred overnight in capped vials, followed by crystallization via slow evaporation of H$_2$O to yield green single crystals. In order to obtain diffraction-quality crystals, it was necessary to recrystallize from acetone. Yield: 0.235 g (95.0%). CCDC 1056650. Anal. Calcd for CuC$_8$H$_{12}$N$_4$Cl$_2$ + 0.05 CuCl$_2$ (%): C, 31.46; H, 3.96; N, 18.35; Cu, 21.85; Cl, 24.38. Found: C, 32.09; H, 3.80; N, 18.50; Cu, 22.23; Cl, 23.88.

2.1.4. *trans*-[Cu(NO$_3$)$_2${4-(CH$_3$)-(C$_3$H$_3$N$_2$)}$_4$] (4). A light blue solution of 0.178 g (0.766 mmol) Cu(NO$_3$)$_2$·2.5 H$_2$O in 4 mL H$_2$O was added via pipette to a colorless 4-methylpyrazole (0.126 g, 1.53 mmol) solution in 5 mL H$_2$O while stirring. A 1 mL rinse of the Cu^{II} vessel with H$_2$O was added to the reaction. An immediate reaction occurred, resulting in a color change to dark royal blue. The reaction was stirred overnight in capped vials, followed by crystallization via slow evaporation of H$_2$O to yield blue-purple single crystals. Yield: 0.190 g (96.4%). CCDC 1056651. Anal. Calcd for CuC$_{16}$H$_{24}$N$_{10}$O$_6$ + 0.025 Cu(NO$_3$)$_2$ (%): C, 36.91; H, 4.65; N, 27.04; Cu, 12.51. Found: C, 37.05; H, 4.52; N, 26.84; Cu, 12.64.

2.1.5. *trans*-[{CuCl[5-(CH$_3$)-(C$_3$H$_3$N$_2$)]$_2$}$_2$(μ-Cl)$_2$] (5). A light blue solution of 0.133 g (0.780 mmol) CuCl$_2$·2H$_2$O in 4 mL H$_2$O was added via pipette to a pale pink 3(5)-methylpyrazole (0.127 g, 1.55 mmol) solution in 5 mL H$_2$O while stirring. A 1 mL rinse of the Cu^{II} vessel with H$_2$O was added to the reaction. An immediate reaction occurred,

resulting in a color change to dark royal blue. The reaction was stirred overnight in capped vials, followed by crystallization via slow evaporation of H_2O to yield green single crystals. Yield: 0.222 g (96.0%). CCDC 1056648. Anal. Calcd for $Cu_2C_{16}H_{24}N_8Cl_4$ + 0.02 $CuCl_2$ (%): C, 31.89; H, 4.01; N, 18.59; Cu, 21.51; Cl, 24.00. Found: C, 31.93; H, 3.95; N, 18.59; Cu, 20.92; Cl, 24.01.

2.1.6. *trans*-[Cu(NO_3)_2{5-(CH_3)-(C_3H_3N_2)}_4] (6). A light blue solution of 0.183 g (0.788 mmol) $Cu(NO_3)_2 \cdot 2.5\ H_2O$ in 4 mL H_2O was added via pipette to a pale pink 3(5)-methylpyrazole (0.128 g, 1.56 mmol) solution in 5 mL H_2O while stirring. A 1 mL rinse of the Cu^{II} vessel with H_2O was added to the reaction. An immediate reaction occurred, resulting in a color change to dark royal blue. The reaction was stirred overnight in capped vials, followed by crystallization via slow evaporation of H_2O to yield blue single crystals. Yield: 0.180 g (89.4%). CCDC 1056652. Anal. Calcd for $CuC_{16}H_{24}N_{10}O_6$ + 0.04 $Cu(NO_3)_2$ (%): C, 36.71; H, 4.62; N, 26.97; Cu, 12.62. Found: C, 36.92; H, 4.58; N, 26.93; Cu, 12.66.

2.1.7. *cis*-[{CuCl[3,5-(CH_3)_2-(C_3H_2N_2)]_2}_2(μ-Cl)_2] (7). A light blue solution of 0.133 g (0.781 mmol) $CuCl_2 \cdot 2H_2O$ in 4 mL H_2O was added via pipette to a white 3,5-dimethylpyrazole (0.149 g, 1.55 mmol) slurry in 5 mL H_2O while stirring. A 1 mL rinse of the Cu^{II} vessel with H_2O was added to the reaction. An immediate reaction occurred, resulting in a color change to green–blue and rapid dissolution of undissolved 3,5-dimethylpyrazole. The reaction was stirred overnight in capped vials, followed by crystallization via slow evaporation of H_2O to yield green single crystals. Yield: 0.239 g (94.5%). CCDC 1056667. Anal. Calcd for $Cu_2C_{20}H_{32}N_8Cl_4$ (%): C, 36.76; H, 4.94; N, 17.15; Cu, 19.45; Cl, 21.70. Found: C, 36.70; H, 4.77; N, 17.17; Cu, 19.43; Cl, 21.70.

2.1.8. [Cu{3,5-(CH_3)_2-(C_3H_2N_2)}_4(H_2O)](NO_3)_2 (8). A light blue solution of 0.180 g (0.773 mmol) $Cu(NO_3)_2 \cdot 2.5\ H_2O$ in 4 mL H_2O was added via pipette to a white 3,5-dimethylpyrazole (0.148 g, 1.54 mmol) slurry in 5 mL H_2O while stirring. A 1 mL rinse of the Cu^{II} vessel with H_2O was added to the reaction. An immediate reaction occurred, resulting in a color change to green–blue and rapid dissolution of undissolved 3,5-dimethylpyrazole. The reaction was stirred overnight in capped vials, followed by crystallization via slow evaporation of H_2O to yield blue-purple single crystals. Yield: 0.215 g (97.7%). CCDC 1056649. Anal. Calcd for $CuC_{20}H_{32}N_{10}O_6$ + 0.05 $Cu(NO_3)_2$ (%): C, 41.31; H, 5.55; N, 24.33; Cu, 11.48. Found: C, 41.87; H, 5.35; N, 24.40; Cu, 11.54.

2.2. *Single-crystal XRD studies*

Diffraction data for each single crystal were collected at 150 K on a 3-circle κ diffractometer equipped with a Bruker APEXII CCD, microfocus Mo κα radiation tube with graphite monochromator, and an Oxford Cryosystems cryostat (except for *trans*-[Cu{4-(CH_3)-(C_3H_3N_2)}_2Cl_2], which was collected at room temperature). Data were processed using the Bruker APEXII software package [4], (data integration and reduction using SAINT [5] and XPREP [6]; multiscan absorption correction using SADABS [7]; structure solution and refinement using SHELXTL [8]). Figures were generated with 50% probability thermal ellipsoids using the X-SEED [9] graphical user interface.

2.3. *Electronic absorption spectroscopy*

Dilute water (0.010 M) and methanol (0.0075 M) solutions were made by dissolving the isolated solid complex into the solvent at room temperature. Though soluble at these concentrations, the complexes were slow to dissolve. The electronic absorption spectra of each solution were measured between 200 and 800 nm (water) or 200–1000 nm (methanol) in 1 cm quartz cuvettes on a Cary 5000 spectrophotometer in dual-beam configuration with neat water or methanol as the reference.

3. Results

3.1. *Synthesis*

Synthesis of the complexes is straightforward. All complexes are soluble in water and none of the complexes precipitate from the reaction until the solvent volume is reduced. Complexes, once crystallized, could be readily redissolved in water. Reaction yields were quantitative assuming the correct stoichiometry (excess Cu^{II} remained in the cases where four-to-one complexes formed but remained in solution upon crystallization).

3.2. *Single-crystal XRD structures*

Structural analysis of the eight synthesized complexes reveals the formation of 4 : 1 ligand: metal complexes, despite the 2 : 1 ligand: metal stoichiometry of the initial reaction, for all of the complexes formed from $Cu(NO_3)_2 \cdot 2.5H_2O$, as well as the complex between $CuCl_2 \cdot 2H_2O$ and pyrazole. All of the complexes between $CuCl_2 \cdot 2H_2O$ and the methylated pyrazoles have two-to-one metal–ligand ratios. Notably, none of the complexes, save **8**, incorporate waters of solvation due to either saturated coordination environments or dense packing in the crystal phase. Structural analysis of individual complexes follows, preceded by the tabulation of crystallographic parameters for the four new structures (table 1).

3.2.1. *trans*-$[Cu(C_3H_4N_2)_4]Cl_2$ (1). Reimann and co-workers [2a] first established the crystal structure of **1** via neutron diffraction, with additional structures by XRD at room temperature reported later [10]. The low-temperature XRD structure acquired during the course of this investigation shows no significant variance from these established structures despite being performed at low temperature, including the two low-temperature structures in the Cambridge Structural Database [11]. Complex **1** crystallizes as purple-blue blocks from water, in the monoclinic space group C2/c at a calculated density of 1.678 g cm^{-3}, with the Cu^{II} center occupying an inversion center. The four coordinated pyrazole ligands are arranged about the Cu^{II} center in a square-planar configuration with the two chloride ions occupying the apical positions in a Jahn–Teller distorted octahedral coordination environment at a distance of 2.82 Å (figure 1, table 2).

Cu^{II}–N distances are 2.00–2.01 Å, typical of Cu^{II}–N distances. Opposing pyrazole ligands are coplanar with one another but inverted through Cu^{II}, with no significant canting of the ligand with respect to the Cl–Cu^{II}–Cl axis. The crystal packing involves intermolecular π–π stacking between pyrazole ligands of neighboring complexes along the crystallographic *c*-axis, forming repeating sets of two mirrored columns of complexes along the

Table 1. Crystal and refinement data for *trans*-[CuCl$_2${4-(CH$_3$)-(C$_3$H$_3$N$_2$)}$_2$] (**3**), *trans*-[Cu(NO$_3$)$_2${4-(CH$_3$)-(C$_3$H$_3$N$_2$)}$_4$] (**4**), *trans*-[{CuCl[5-(CH$_3$)-(C$_3$H$_3$N$_2$)]$_2$}$_2$(μ-Cl)$_2$] (**5**), and *trans*-[Cu(NO$_3$)$_2${5-(CH$_3$)-(C$_3$H$_3$N$_2$)}$_4$] (**6**).

| Complex	3	4	5	6
Empirical formula	C$_8$H$_{12}$Cl$_2$CuN$_4$	C$_{16}$H$_{24}$CuN$_{10}$O$_6$	C$_8$H$_{12}$Cl$_2$CuN$_4$	C$_{16}$H$_{24}$CuN$_{10}$O$_6$
Formula weight	298.66	515.99	298.66	515.99
Crystal size (mm^3)	0.22 × 0.04 × 0.01	0.25 × 0.21 × 0.03	0.35 × 0.14 × 0.08	0.49 × 0.21 × 0.06
T (K)	296(2)	150(2)	150(2)	150(2)
λ (Å)	0.71073	0.71073	0.71073	0.71073
Crystal system	Monoclinic	Monoclinic	Monoclinic	Monoclinic
Space group	P2$_1$/n	P2$_1$/c	P2$_1$/n	P2$_1$/n
a (Å)	4.8025(18)	9.3280(17)	7.4990(8)	9.2867(5)
b (Å)	17.418(6)	9.1948(11)	8.7494(10)	8.6815(5)
c (Å)	7.141(3)	13.6751(17)	17.833(2)	14.4137(9)
α (°)	90	90	90	90
β (°)	91.378(5)	98.527(7)	98.989(5)	108.788(2)
γ (°)	90	90	90	90
V (Å^3)	597.2(4)	1159.9(3)	1155.7(2)	1100.15(11)
Z	2	2	4	2
ρ_{calc} (g cm^{-3})	1.661	1.477	1.716	1.558
μ (mm^{-1})	2.248	0.995	2.324	1.049
$F(0\,0\,0)$	302	534	604	534
θ range (°)	2.339–27.654	2.21–28.35	2.31–29.17	2.32–28.30
hkl range	$-5 \leq h \leq 6$ $-22 \leq k \leq 22$ $-9 \leq l \leq 9$	$-12 \leq h \leq 12$ $-12 \leq k \leq 12$ $-18 \leq l \leq 17$	$-10 \leq h \leq 9$ $-12 \leq k \leq 12$ $-5 \leq l \leq 24$	$-12 \leq h \leq 12$ $-11 \leq k \leq 11$ $-19 \leq l \leq 18$
Reflections collected	5481	12,549	9174	10,202
Independent reflections	1374	2875	3031	2742
Completeness to $\theta = 25.00°$	100.0	99.4	98.8	100.0 %
Data/restraints/parameters	1374/0/94	2875/0/153	3031/0/139	2742/0/153
Goodness of fit on F^2	1.048	0.995	1.178	1.047
Final R indices [$I > 2\sigma(I)$]	$R_1 = 0.0368$ $wR_2 = 0.0797$	$R_1 = 0.0320$ $wR_2 = 0.0849$	$R_1 = 0.0455$ $wR_2 = 0.1292$	$R_1 = 0.0322$ $wR_2 = 0.0915$
R indices (all data)	$R_1 = 0.0577$ $wR_2 = 0.0881$	$R_1 = 0.0432$ $wR_2 = 0.0886$	$R_1 = 0.0520$ $wR_2 = 0.1325$	$R_1 = 0.0393$ $wR_2 = 0.0939$
Largest diff. peak, hole (e Å^{-3})	0.734, −0.256	0.399, −0.508	0.772, −1.569	0.476, −0.540
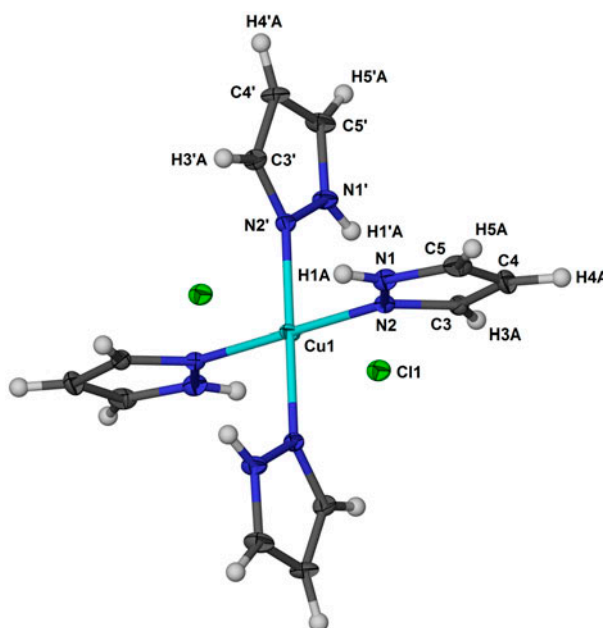
Figure 1.   Structure of *trans*-[Cu(C$_3$H$_4$N$_2$)$_4$]Cl$_2$ (**1**) with ellipsoids drawn at the 50% probability level; atom colors are teal (Cu), blue (N), gray (C), green (Cl), and white (H) (see http://dx.doi.org/10.1080/00958972.2015.1077952 for color version).

Table 2.   Coordination environment bond lengths (Å) for complexes **1–8**; N$_{pz}$ is the pyrazole nitrogen in the 2-position, (s) denotes the short Cu–N$_{pz}$ bond, (l) denotes the long Cu–N$_{pz}$ bond, (t) denotes terminal Cu–Cl bond, (sb) denotes the short bridging Cu–Cl bond, (lb) denotes the long bridging Cu–Cl bond.

	1	**2**	**3**	**4**	**5**	**6**	**7**	**8**
Cu–N$_{pz}$ (s)	2.002(2)	1.998(2)	1.991(3)	2.008(1)	1.995(3)	1.997(1)	1.987(9)	1.991(1)
Cu–N$_{pz}$ (l)	2.014(2)	2.011(2)	–	2.014(1)	1.998(3)	2.023(1)	2.013(8)	2.035(1)
Cu–ONO$_2$	–	2.410(2)	–	2.344(1)	–	2.370(1)	–	–
Cu–OH$_2$	–	–	–	–	–	–	–	2.165(2)
Cu–Cl (t)	–	–	2.275(1)	–	2.281(1)	–	2.299(3)	–
Cu–Cl (sb)	–	–	–	–	2.318(1)	–	2.324(3)	–
Cu–Cl (lb)	–	–	–	–	2.729(1)	–	2.663(3)	–

crystallographic *b*-axis (figure 2), with slight canting of the complex to accommodate the ligand interactions. Hydrogen bonding between Cl$^-$ and the pyrazole N–H proton occurs with a Cl–H distance of 2.46 Å.

3.2.2.   *trans*-[Cu(NO$_3$)$_2$(C$_3$H$_4$N$_2$)$_4$] (2).

Yamaguchi and co-workers previously reported the room-temperature XRD structure of **2**, which crystallizes as purple-blue blocks in the monoclinic C2/c space group [2b]. The low-temperature structure reported herein deviates only slightly from the established structure, primarily with regard to unit cell size, which is smaller in the low-temperature structure, and thus, a higher calculated density of 1.698 g cm^{-3} is observed. The structure of **2** itself is similar to **1** above, comprising a Jahn–Teller distorted six-coordinate Cu^{II} center occupying an inversion center and pyrazole
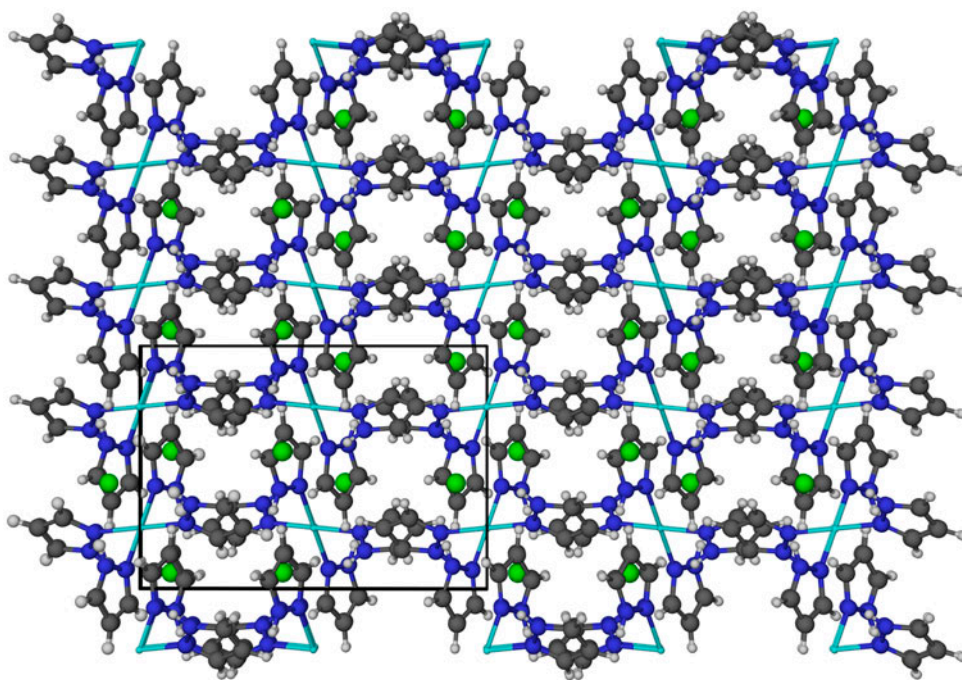
Figure 2.   Packing of *trans*-[Cu(C$_3$H$_4$N$_2$)$_4$]Cl$_2$ (**1**) as viewed down the crystallographic *a*-axis with the unit cell inscribed in black (*b*-axis along the vertical, *c*-axis along the horizontal), highlighting the canting of individual complexes, the sets of mirrored columns, and the π–π stacking along the *c*-axis.

ligands arranged in a similar manner, with Cu^{II}–N distances of 2.00 Å and 2.01 Å. The two nitrate anions coordinate through an oxygen, with a Jahn–Teller elongated Cu^{II}–O distance of 2.41 Å (figure 3, table 2). The pyrazole ligands, unlike **1**, are canted 10° (hydrogen bonded to nitrate) and 13° (not hydrogen bonded) with respect to the O–Cu^{II}–O axis, and the nitrate ions are tilted 45° from linear.

Again, intermolecular π–π stacking of the ligands guides the packing, occurring along the crystallographic *b*-axis. Along the crystallographic *b*-axis, pyrazole ligands from different complexes are tilted ~80° with respect to one another (figure 4). Intramolecular hydrogen bonding occurs between H1A and H3′A (pyrazole N–H) and the nitrate O3 and O2, respectively, with an O–H distance of 2.02 Å in each case.

3.2.3. *trans*-[CuCl$_2${4-(CH$_3$)-(C$_3$H$_3$N$_2$)}$_2$] (3). Due to difficulty in obtaining a suitable crystal for XRD measurements via slow evaporation of water, **3** was crystallized by dissolution in and slow evaporation from acetone. The square-planar complex crystallizes in the monoclinic P2$_1$/n space group as green needles at a calculated density of 1.661 g cm^{-3}. Complex **3** comprises a discrete monomer with a four-coordinate square-planar Cu^{II} center occupying an inversion center, with two pyrazole ligands trans-coordinated at a Cu^{II}–N distance of 1.99 Å and two chlorides trans-coordinated at a Cu^{II}–Cl distance of 2.27 Å (figure 5, table 2). Unlike the other complexes described herein, **3** contains only four coordinated moieties. The pyrazole ligands are coplanar but inverted through the Cu^{II} center and rotated 11° out of plane with respect to the Cu^{II} coordination environment.
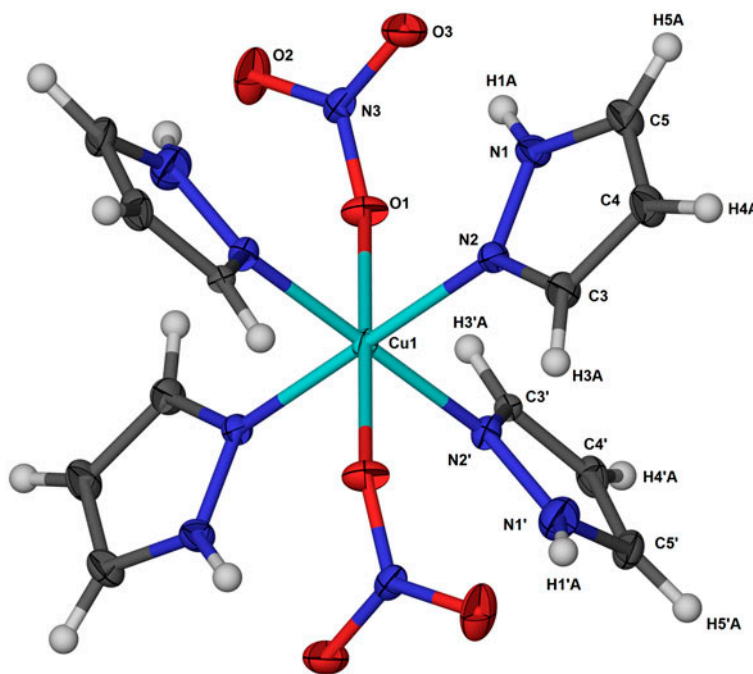
Figure 3. Structure of *trans*-[Cu(NO$_3$)$_2$(C$_3$H$_4$N$_2$)$_4$] (**2**) with ellipsoids drawn at the 50% probability level; atom colors are teal (Cu), blue (N), gray (C), red (O), and white (H) (see http://dx.doi.org/10.1080/00958972.2015.1077952 for color version).

Complex **3** packs in a herringbone fashion, with the 4-methylpyrazole ligands located above the neighboring Cu^{II} ion rather than another 4-methylpyrazole ligand (figure 6). The methyl substituents pack in an interlocking manner between opposing columns of complexes. Intramolecular hydrogen bonding occurs between H1A and Cl1, with a distance of 2.48 Å.

3.2.4. ***trans*-[Cu(NO$_3$)$_2$\{4-(CH$_3$)-(C$_3$H$_3$N$_2$)\}$_4$] (4).** Isolated as blue-purple blocks from water, **4** packs in the monoclinic P2$_1$/c space group at a calculated density of 1.477 g cm^{-3}. The structure of the complex itself is reminiscent of **2**. The six-coordinate Cu^{II} ion lies on an inversion center, with four 4-methylpyrazole ligands arranged in a square plane and two nitrates occupying the apical positions of the octahedral environment (figure 7). The Cu^{II}–N distances are 2.01 Å while the Cu^{II}–O distances are 2.34 Å due to Jahn–Teller distortion (table 2). As in **2**, opposing pyrazole ligands are coplanar with one another but inverted through Cu^{II}. Similar ligand canting with respect to the O–Cu^{II}–O axis occurs, though at a higher angle of 19° for the ligands engaged in hydrogen bonding with the coordinated anion and an even greater 37° for those that are not. The nitrate ligands are also tilted to a greater degree, 51° from linear.

Complex **4** packs in a corrugated manner along the crystallographic *b*-axis, with the ligand methyl groups and nitrates occupying the interstices between the complexes (figure 8). No intermolecular π–π stacking between the ligands occurs. Intramolecular hydrogen bonding between H1′A and O3 occurs with a distance of 2.06 Å.
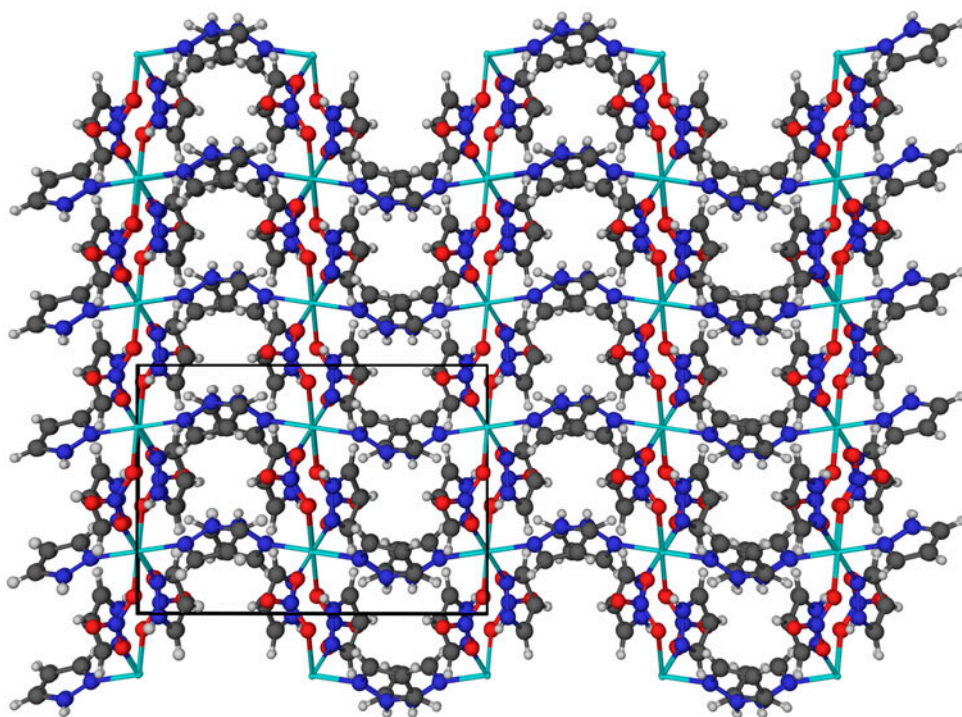
Figure 4. Packing of *trans*-[Cu(NO$_3$)$_2$(C$_3$H$_4$N$_2$)$_4$] (**2**) as viewed down the crystallographic *a*-axis with the unit cell inscribed in black (*b*-axis along the vertical, *c*-axis along the horizontal), highlighting canting of individual complexes, sets of mirrored columns, and π–π stacking along the *c*-axis similar to that of **1**.
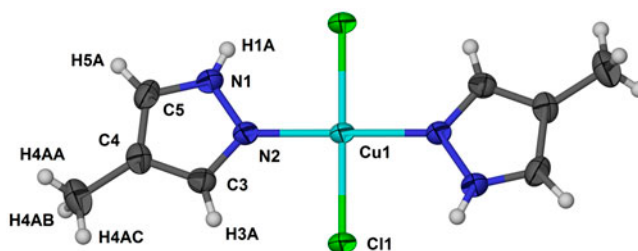

Figure 5. Structure of *trans*-[CuCl$_2${4-(CH$_3$)-(C$_3$H$_3$N$_2$)}$_2$] (**3**) with ellipsoids drawn at the 50% probability level. Atom colors are teal (Cu), blue (N), gray (C), green (Cl), and white (H) (see http://dx.doi.org/10.1080/00958972.2015.1077952 for color version).

3.2.5. *trans*-[{CuCl[5-(CH$_3$)-(C$_3$H$_3$N$_2$)]$_2$}$_2$(μ-Cl)$_2$] (5).

Green blocks of **5** crystallize from the slow evaporation of water, packing in the monoclinic P2$_1$/n space group at a calculated density of 1.716 g cm^{-3}. The structure is reminiscent of that observed for **3** (with 4-methylpyrazole as the ligand); however, the 5-methylpyrazole congener forms discrete dimers bridged by chloride. The 5-methylpyrazole ligands are trans-coordinated about a locally five-coordinate square-pyramidal Cu^{II} center, deflected by 8° away from the basal
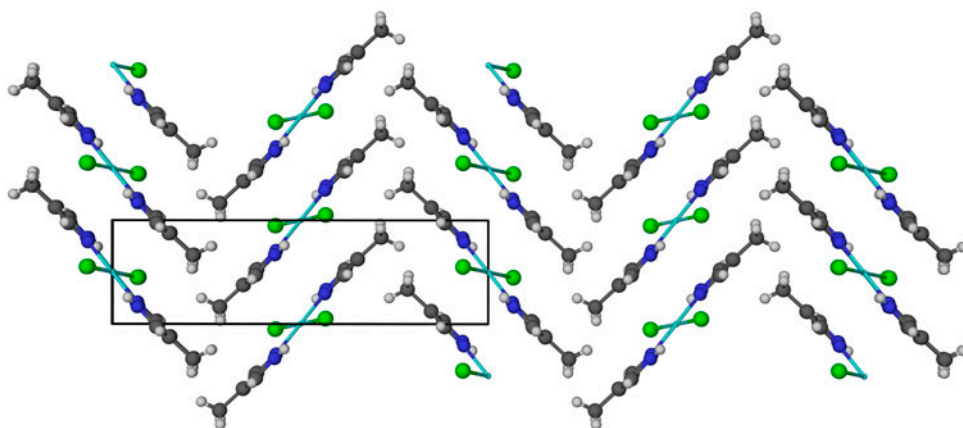
Figure 6. Packing of *trans*-[CuCl$_2$\{4-(CH$_3$)-(C$_3$H$_3$N$_2$)\}$_2$] (**3**) as viewed down the crystallographic *c*-axis with the unit cell inscribed in black (*a*-axis along the vertical, *b*-axis along the horizontal), highlighting the herringbone-style packing of the individual complexes and the interlocking methyl groups along the *a*-axis.
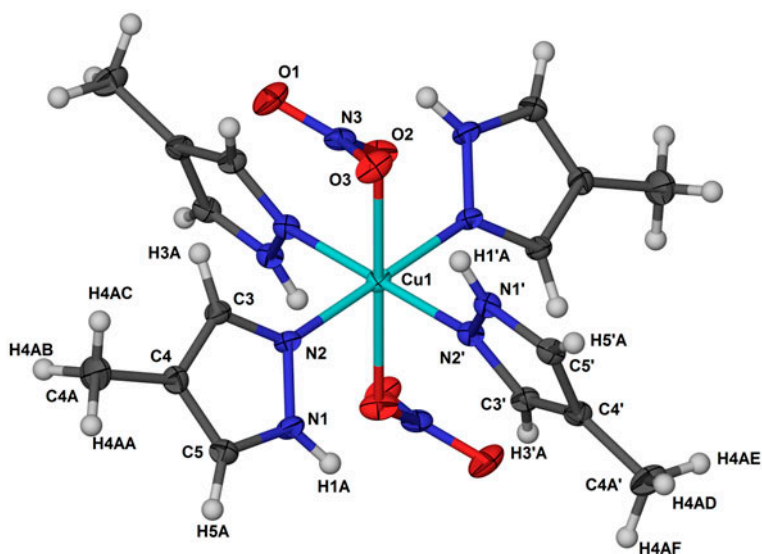

Figure 7. Structure of *trans*-[Cu(NO$_{-3}$)$_2$\{4-(CH$_3$)-(C$_3$H$_3$N$_2$)\}$_4$] (**4**) with ellipsoids drawn at the 50% probability level. Atom colors are teal (Cu), blue (N), gray (C), red (O), and white (H) (see http://dx.doi.org/10.1080/00958972.2015.1077952 for color version).

plane, and canted slightly, with Cu^{II}–N distances of 2.00 Å for both ligands (figure 9). The chlorides in the base of the local Cu^{II} square-pyramidal coordination environment are also deflected 10° from the basal plane, with Cu^{II}–Cl distances of 2.28 and 2.32 Å for the terminal and bridging chlorides, respectively. The apical position is occupied by a chloride bridging from the other half of the dimer, with a Jahn–Teller distorted distance of 2.73 Å (notably shorter than the 2.82 Å Cu^{II}–Cl distance in the pyrazole congener described above). Coordination environment bond lengths are located in table 2.
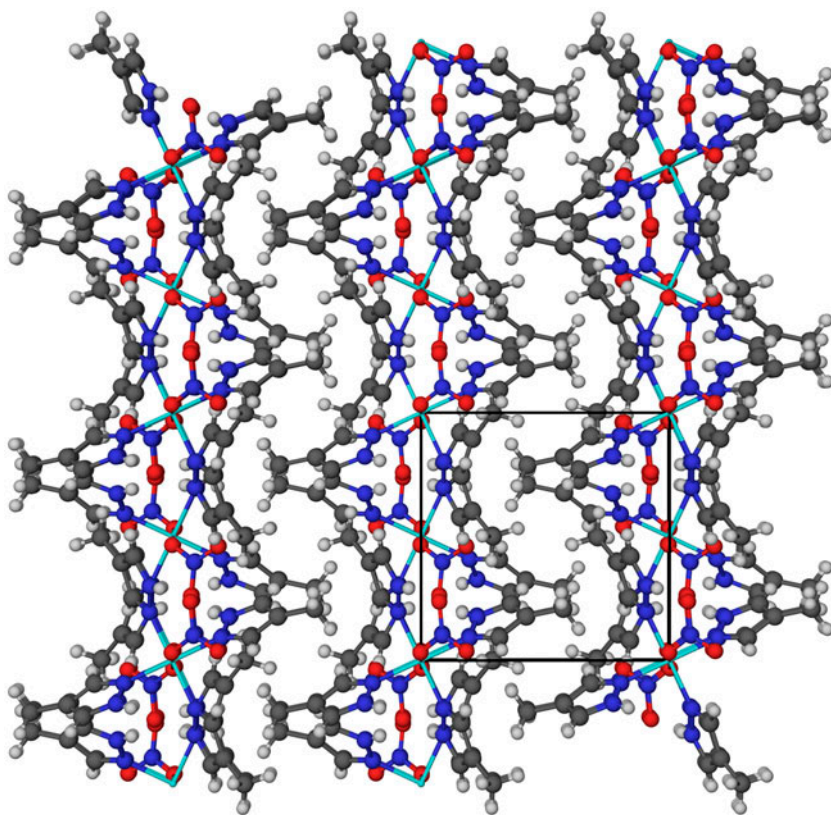
Figure 8. Packing of *trans*-[Cu(NO-$_3$)$_2${4-(CH$_3$)-(C$_3$H$_3$N$_2$)}$_4$] (**4**) as viewed down the crystallographic *c*-axis with the unit cell inscribed in black (*b*-axis along the vertical, *a*-axis along the horizontal), highlighting the slight corrugation along the *b*-axis and the "channels" of methyl groups in the interstices.
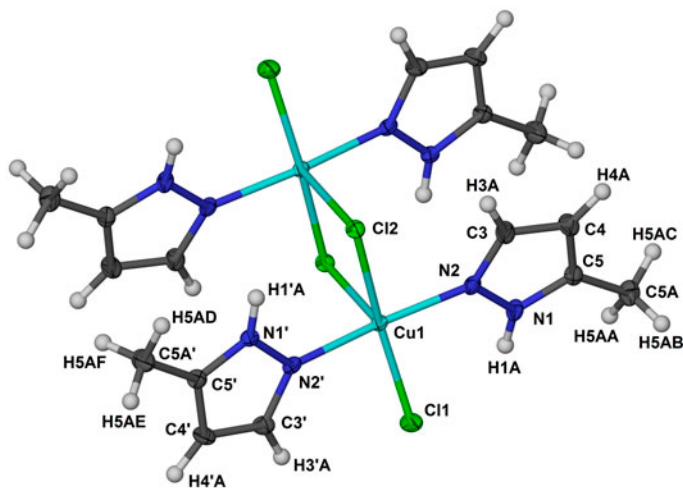
Figure 9. Structure of *trans*-[{CuCl[5-(CH$_3$)-(C$_3$H$_3$N$_2$)]$_2$}$_2$(μ-Cl)$_2$] (**5**) with ellipsoids drawn at the 50% probability level; atom colors are teal (Cu), blue (N), gray (C), green (Cl), and white (H) (see http://dx.doi.org/10.1080/00958972.2015.1077952 for color version).

The dimers pack in a herringbone pattern similar to that seen for **3** along the crystallographic *c*-axis (figure 10). There is no intramolecular π–π stacking despite the close association of pyrazole ligands, which deflect away from one another in the dimers. There is also no intermolecular π–π stacking within or between the columns composing the herringbone packing. Hydrogen bonding occurs between both chloride ions and pyrazole N–H groups, with distances of 2.43 Å for H1′A-Cl2 and 2.53 Å for H1A-Cl1.

3.2.6. *trans*-**[Cu(NO$_3$)$_2$\{5-(CH$_3$)-(C$_3$H$_3$N$_2$)\}$_4$] (6).** Purple-blue prisms of **6** crystallize from water upon slow evaporation, with the complex packing in the monoclinic P2$_1$/n space group at a calculated density of 1.557 g cm^{-3} (table 2 lists coordination environment bond lengths). In a manner similar to the pyrazole and 4-methylpyrazole congeners **2** and **4**, the complex comprises a six-coordinate Cu^{II} center occupying an inversion center with four 5-methylpyrazole ligands arranged in a square plane and two nitrates occupying the apical positions of the octahedral environment (figure 11). The 5-methylpyrazole ligands not participating in intramolecular hydrogen bonding with the nitrate anions are canted with respect to the O–Cu^{II}–O axis by 26°, while the hydrogen bonding ligands are canted by only 7°. The N–Cu^{II} distances are 2.00 and 2.02 Å for the hydrogen-bonded and non-hydrogen-bonded pyrazole ligands, respectively. The nitrate O–Cu^{II} distance is 2.37 Å due to Jahn–Teller elongation. The nitrates are also deflected away from the plane by 48°.

Complex **6** packs in offset columns running along the crystallographic *b*-axis (figure 12). The methyl groups of the ligand and the loosely coordinated nitrates occupy the interstices
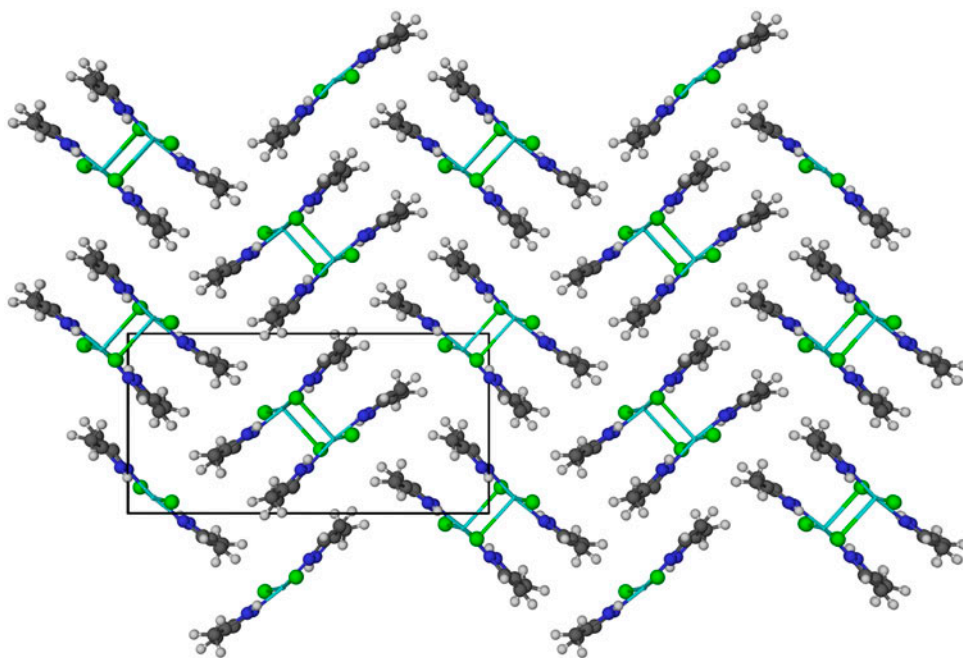
Figure 10. Packing of *trans*-[\{CuCl[5-(CH$_3$)-(C$_3$H$_3$N$_2$)]$_2$\}$_2$(μ-Cl)$_2$] (**5**) as viewed down the crystallographic *a*-axis with the unit cell inscribed in black (*b*-axis along the vertical, *c*-axis along the horizontal), highlighting the herringbone-style packing of the dimers.
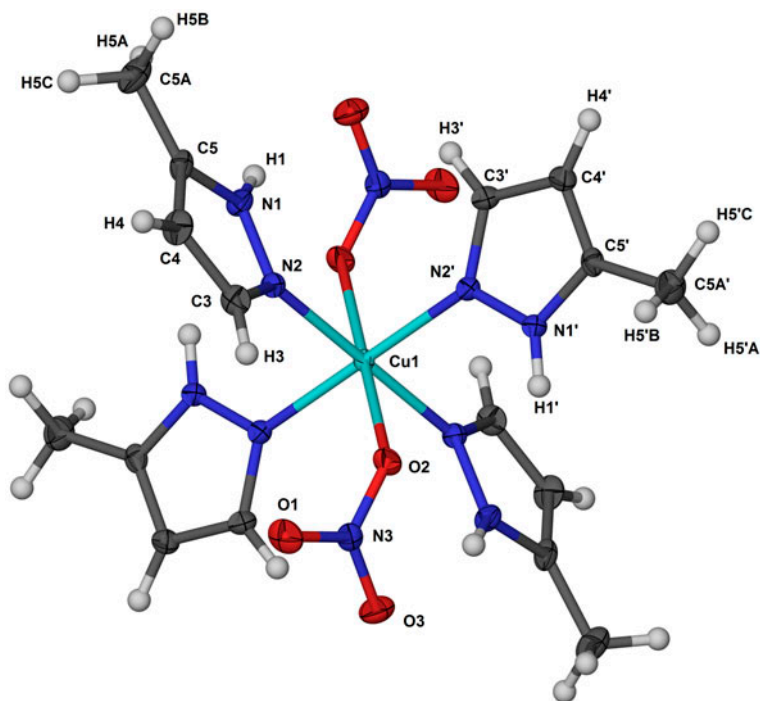
Figure 11. Structure of *trans*-[Cu(NO$_3$)$_2$\{5-(CH$_3$)-(C$_3$H$_3$N$_2$)\}$_4$] (**6**) with ellipsoids drawn at the 50% probability level; atom colors are teal (Cu), blue (N), gray (C), red (O), and white (H) (see http://dx.doi.org/10.1080/00958972.2015.1077952 for color version).

between the columns. Hydrogen bonding between the nitrate anions and only two of the four 5-methylpyrazole ligand N–H atoms occurs at a distance of 2.26 Å.

3.2.7. *cis*-[\{CuCl[3,5-(CH$_3$)$_2$-(C$_3$H$_2$N$_2$)]\}$_2$\}$_2$(μ-Cl)$_2$] (7). The structure of **7** was first established by Rheingold and co-workers, although it was isolated from an anhydrous dichloromethane/hexane recrystallization of a product resulting from the degradation of (CH$_3$)P(S)(3,5-(CH$_3$)$_2$-C$_3$H$_2$N$_2$)$_2$ and anhydrous CuCl$_2$ [3a], not an aqueous reaction between 3,5-dimethylpyrazole itself and CuCl$_2$·2H$_2$O as presented herein. The bridged dimer **7** crystallizes as green rods in the space group P-1 with a calculated density of 1.63 g cm^{-3} from slowly evaporated water solutions.

The local coordination environment about each Cu^{II} ion in **7** is a five-coordinate square-pyramid comprising a base of two 3,5-dimethylpyrazole ligands cis-coordinated, a terminal Cl$^-$, and the shorter of two bridging Cl$^-$ ion bonds, while the apical position is occupied by the elongated contact between Cu^{II} and the other bridging Cl$^-$ (figure 13). Cu^{II}–N distances are slightly different based on location in the coordination environment, with a Cu^{II}–N distance of 2.00 Å for the ligand trans to the terminal Cl$^-$ and 2.03 Å for the ligand trans to the bridging Cl$^-$. The terminal Cl$^-$ has the shortest bond, with a Cu^{II}–Cl distance of 2.30 Å, while the Cu^{II}–Cl distances for the bridging chlorides are 2.32 and 2.67 Å for the basal and apical Cu^{II}–Cl bonds, respectively. Coordination bond lengths are listed in table 2.
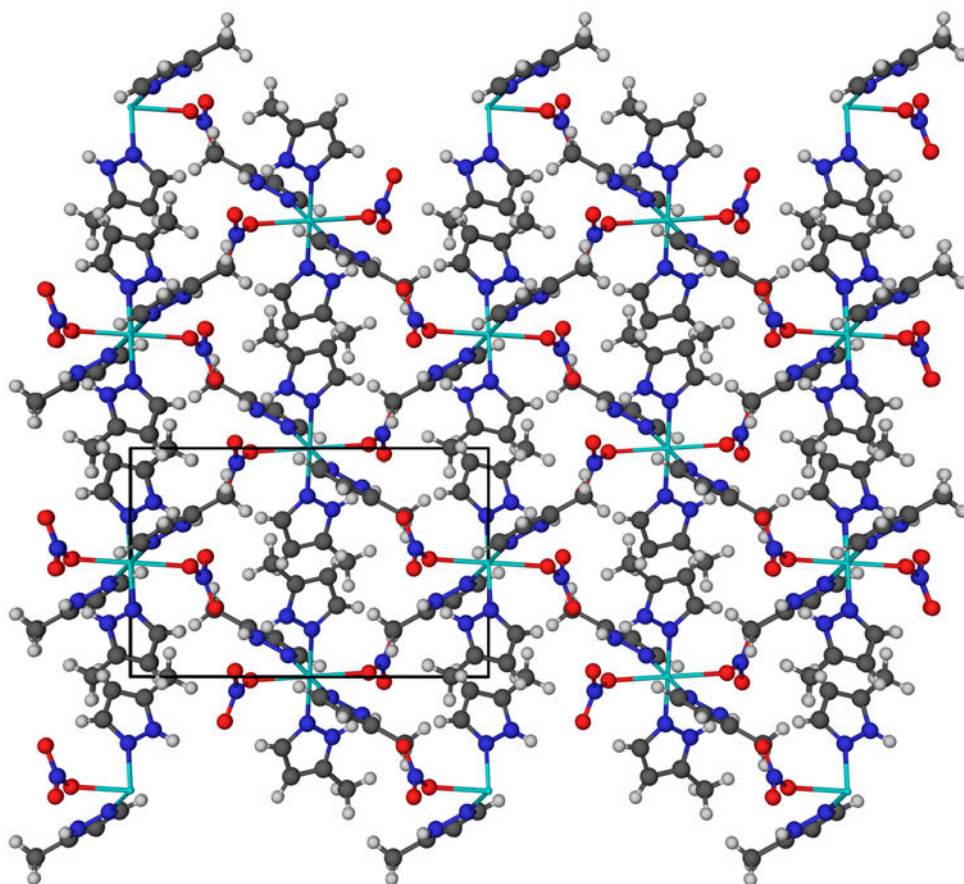
Figure 12. Packing of *trans*-[Cu(NO$_3$)$_2${5-(CH$_3$)-(C$_3$H$_3$N$_2$)}$_4$] (**6**) as viewed down the crystallographic *a*-axis with the unit cell inscribed in black (*b*-axis along the vertical, *c*-axis along the horizontal), highlighting the offset columns running along the *b*-axis and the "channels" of methyl and nitrate groups in the interstices.

Unlike the 4-methyl- and 5-methylpyrazole congeners **3** and **5**, **7** packs in staggered interlocked columns of dimers, not a herringbone pattern (figure 14). The ligands do not participate in any inter- or intramolecular π–π stacking interactions. There are no interstitial water molecules included within the structure. The dimer also exhibits intramolecular hydrogen bonding between the terminal chloride of one Cu^{II} center and the N–H proton of the ligand on the second Cu^{II} center opposing the terminal chloride at a Cu^{II}–Cl distance of 2.33 Å.

3.2.8. [Cu{3,5-(CH$_3$)$_2$-(C$_3$H$_2$N$_2$)}$_4$(H$_2$O)](NO$_3$)$_2$ (8). The structure of **8** was first established by Lavrenova and co-workers, although their structure was determined at room temperature on material repeated by recrystallized from ethanol [3b]. Related structures of the complex formed between Cu(NO$_3$)$_2$·2.5H$_2$O and 3,5-dimethylpyrazole have been determined by Ziegler *et al.* [12], Tomaskiewicz *et al.* [13], and Reedijk *et al.* [14], although in each of these cases, only three 3,5-dimethylpyrazole ligands coordinate to the Cu^{II} center and the nitrate anions remain coordinated as a result of either using trimethyl- or triethylorthoformate
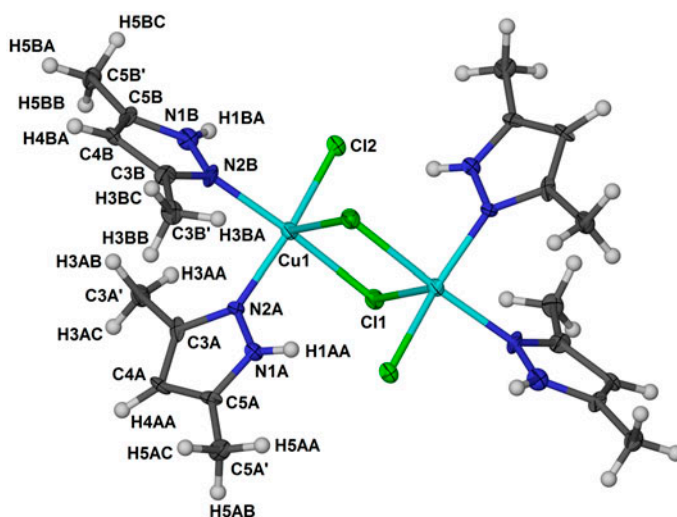
Figure 13. Structure of *cis*-[{CuCl[3,5-(CH$_3$)$_2$-(C$_3$H$_2$N$_2$)]$_2$}$_2$(μ-Cl)$_2$] (**7**) with ellipsoids drawn at the 50% probability level; atom colors are teal (Cu), blue (N), gray (C), green (Cl), and white (H) (see http://dx.doi.org/10.1080/00958972.2015.1077952 for color version).

as a dehydrating agent (Tomaskiewicz [13] and Reedijk [14], respectively) or recrystallization from CH$_2$Cl$_2$ (Ziegler [12]).

When the reaction is performed in and the product crystallized from water, a structure similar to that of Lavrenova and co-workers is isolated, crystallizing as blue blocks with a calculated density of 1.42 g cm^{-3} in the space group C2/c, as determined by low-temperature XRD. The Cu^{II} center resides on a twofold axis in a five-coordinate square-pyramidal coordination environment, elevated slightly from the basal plane (figure 15). The basal plane comprises four 3,5-dimethylpyrazole ligands arranged such that two opposing 3,5-dimethylpyrazole ligand N–H bonds point toward the pyramid apex and the two others point away, with Cu^{II}–N distances of 1.99 and 2.03 Å, respectively (table 2). The apical position is occupied by a water molecule at a Cu^{II}–O distance of 2.17 Å. Unlike all other complexes reported herein, the nitrate ions in **8** are not directly coordinated to the Cu^{II} center but rather reside in the outer coordination sphere within a hydrogen bonding network, including the pyrazole N–H, NO$_3^-$ and the coordinated water molecule (*vide infra*).

Complex **8** packs in columnar stacks along the crystallographic *b*-axis, with adjacent columns stacking in opposite directions (figure 16). Adjacent columns are offset by 1/4 along the crystallographic *c*-axis. Extensive hydrogen bonding occurs between the ligand N–H and the nitrates at O–H distances of 1.97 and 1.99 Å for the N–H bonds pointed away from and toward the apical water molecule, respectively. The coordinated water also engages in a hydrogen bond with the nitrates at an O–H distance of 1.86 Å. All three oxygen atoms of each nitrate are hydrogen bonded to different protons in the complex, influencing not only the nitrate orientation but the water and ligand orientations as well.

3.3. *Spectroscopy*

Electronic absorption spectroscopy of the complexes in water exhibits two distinct absorption bands – one in the low-energy visible and one in the UV (figure 17). These bands are
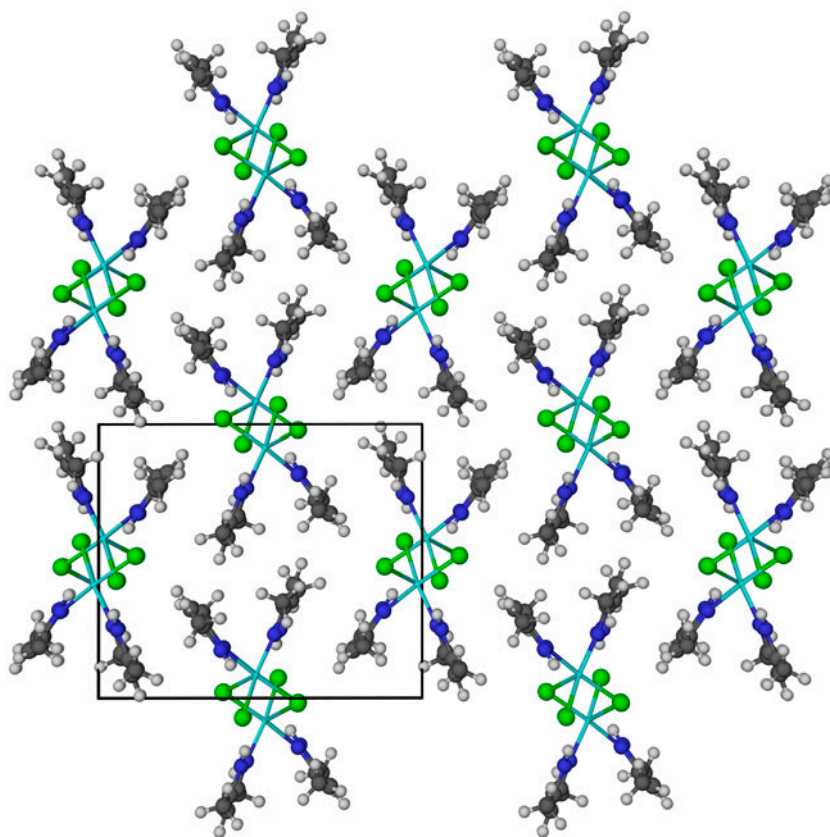
Figure 14. Packing of *cis*-[{CuCl[3,5-(CH$_3$)$_2$-(C$_3$H$_2$N$_2$)]$_2$}$_2$(μ-Cl)$_2$] (**7**) as viewed down the crystallographic *a*-axis with the unit cell inscribed in black (*b*-axis along the vertical, *c*-axis along the horizontal), highlighting the interlocked columns of **7**.

assigned, respectively, to the Cu^{II} d–d transition and LMCT between the ligand π orbital and Cu^{II}, based on observed extinction coefficients, previous work by Bernaducci *et al.* [15], and reported pyrazole ligand UV absorption bands [16], which are higher in energy than those observed. The Cu^{II} d–d transitions are all broad, weak absorptions between 680 and 740 nm, their respective absorption wavelengths depending both on the coordinated ligand and counterion. Complexes **1–6** all exhibit bands in the UV region at 310 nm, with higher energy shoulders at ~270 nm. Complexes **7** and **8** (with 3,5-dimethylpyrazole) exhibit only a single band near 310 nm.

There is little difference in the ligand UV absorption bands between the nitrate and chloride complexes of pyrazole (**1** and **2**). For **3–8**, however, the extinction coefficient for the UV bands in the nitrate complexes is approximately twice that of the chloride complexes, consistent with the difference in ligand to metal (L : M) ratio between nitrate and chloride complexes (4 : 1 L : M and 2 : 1 L : M, respectively). This, coupled with observations in the visible region upon changing solvent (*vide infra*), demonstrates that the ligands do not dissociate from Cu^{II} in water or methanol. Upon subsequent addition of electron-donating substituents to the pyrazole ligand, a bathochromic shift of the UV band occurs.
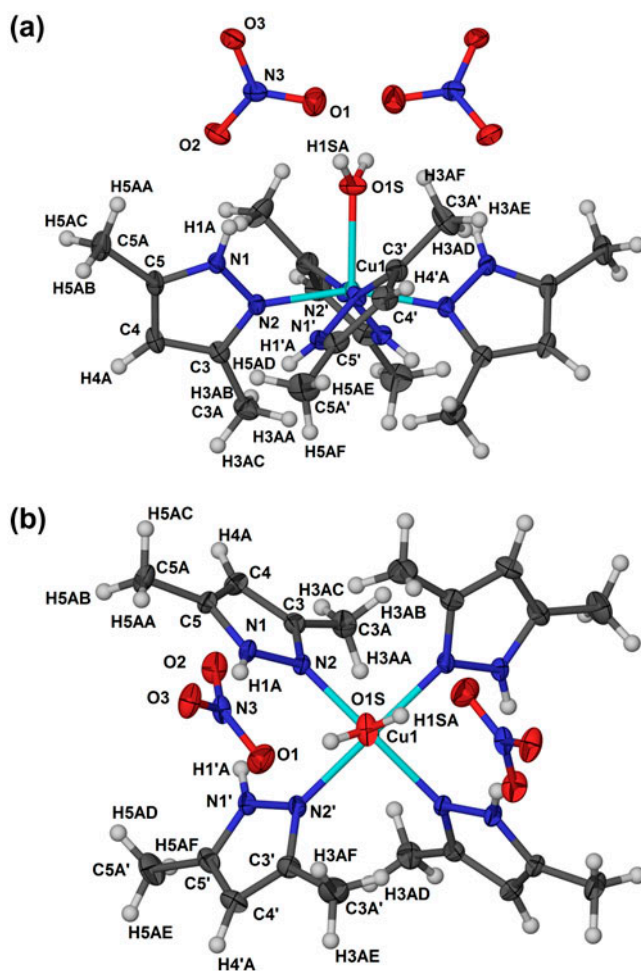
Figure 15.   Side view (a) and top view (b) of the structure of $[Cu\{3,5\text{-}(CH_3)_2\text{-}(C_3H_2N_2)\}_4(H_2O)](NO_3)_2$ (8) with ellipsoids drawn at the 50% probability level; atom colors are teal (Cu), blue (N), gray (C), red (O), and white (H) (see http://dx.doi.org/10.1080/00958972.2015.1077952 for color version).

The visible bands observed for the nitrate complexes of the methylated pyrazoles are, with the exception of 4, located close to one another at 700 nm (6) and 706 nm (8) in water solution. Complex 4, however, undergoes a significant hypsochromic shift to 680 nm, the highest energy visible absorption of all of the complexes. A similar trend is observed in the chloride complexes of the methylated pyrazoles (3, 5, 7), although the shift is not as dramatic (730 nm for 3 *versus* 745 nm and 739 nm for 5 and 7, respectively). Also, the wavelength of the visible absorption bands for the nitrate complexes is generally higher in energy than those for the chloride complexes. Spectra in methanol (figure 18) show a bathochromic shift for the visible bands of 3, 5, and 7 but little change for the nitrate complexes 4, 6, and 8.
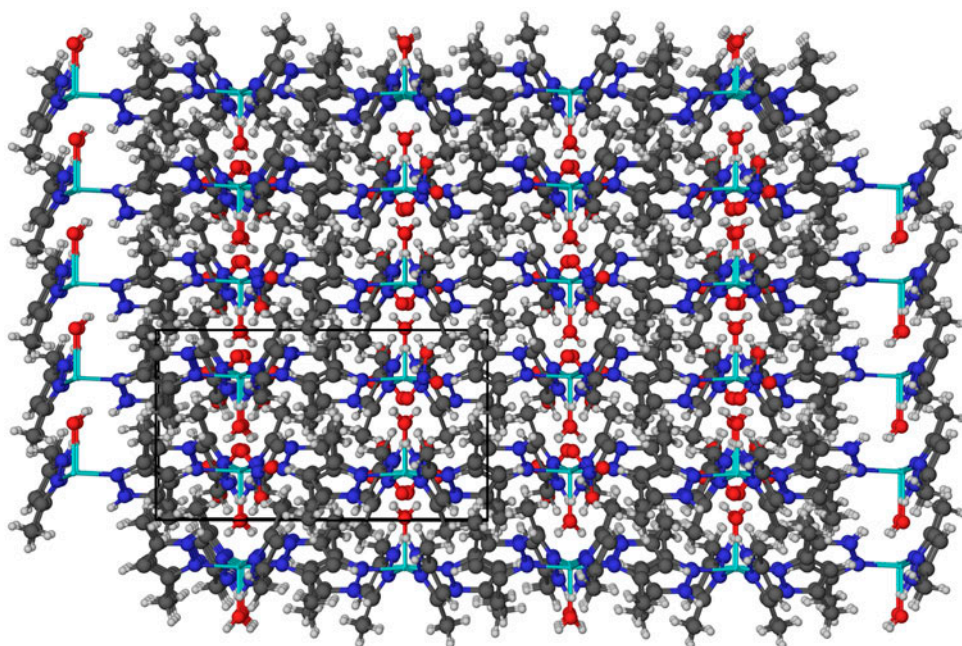
Figure 16. Packing of $[Cu\{3,5\text{-}(CH_3)_2\text{-}(C_3H_2N_2)\}_4(H_2O)](NO_3)_2$ (**8**) as viewed down the crystallographic *a*-axis with the unit cell inscribed in black (*b*-axis along the vertical, *c*-axis along the horizontal), highlighting the columnar stacks of **8**.

Figure 17. UV–visible spectra of 0.010 M water solutions of **1** (red solid line), **2** (red dashed line), **3** (teal solid line), **4** (teal dashed line), **5** (purple solid line), **6** (purple dashed line), **7** (green solid line), and **8** (green dashed line). Inset shows an expanded view of the visible region. Chloride complexes are all represented by solid lines, nitrate complexes by dashed lines (see http://dx.doi.org/10.1080/00958972.2015.1077952 for color version).

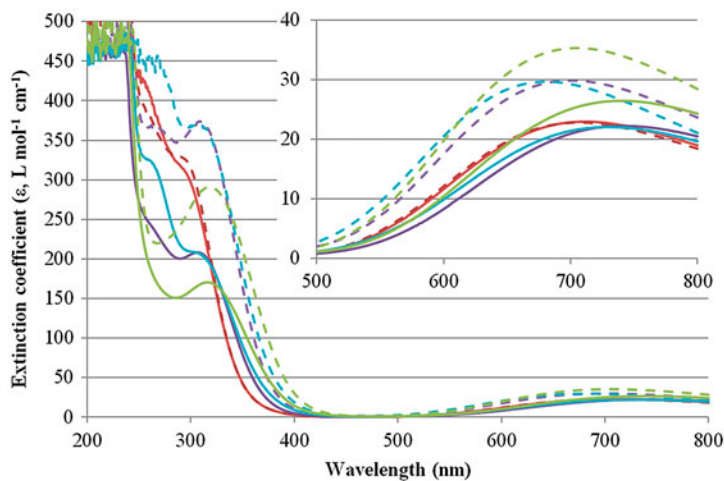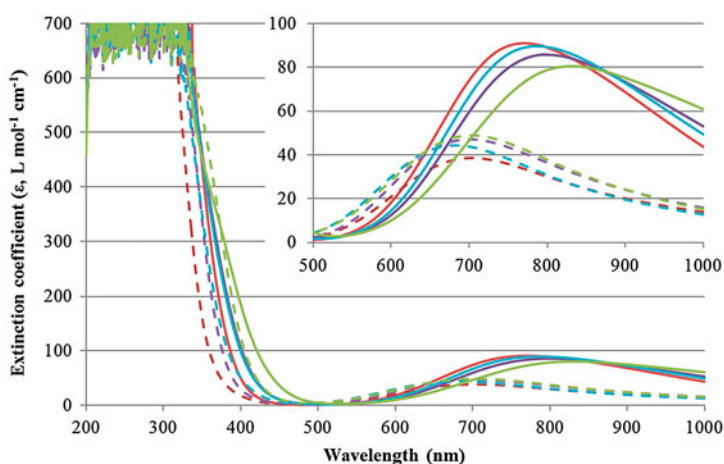Figure 18. UV–visible spectra of 0.0075 M methanol solutions of **1** (red solid line), **2** (red dashed line), **3** (teal solid line), **4** (teal dashed line), **5** (purple solid line), **6** (purple dashed line), **7** (green solid line), and **8** (green dashed line). Inset shows an expanded view of the visible region. Chloride complexes are all represented by solid lines, nitrate complexes by dashed lines (see http://dx.doi.org/10.1080/00958972.2015.1077952 for color version).

4. Discussion

4.1. *Structural trends*

Despite similar reaction conditions, the small differences in methyl substituent placement and counterion coordination strength have significant effects on the final structures of the resulting complexes. The Cu^{II}–N distances of all complexes measure 2.01 ± 0.02 Å, with Cu^{II}–Cl and Cu^{II}–ONO_2 bonds varying more due to varying extents of Jahn–Teller distortion; Cu^{II}–Cl distances range between 2.27 and 2.73 Å while Cu^{II}–ONO_2 distances range between 2.34 and 2.41 Å. The wider range of Cu^{II}–Cl bonds as compared to Cu^{II}–ONO_2 bonds is attributed to the presence of bridging Cl^- in two of the complexes and the greater diffusion of charge over the larger nitrate anion.

With nitrate as the counterion, complexes containing a 4 : 1 ligand : metal ratio form, regardless of steric hindrance from the ligands. In the case of **8**, however, the Cu^{II} center is five-coordinate and the nitrates are relegated to the outer coordination sphere due to methyl groups completely blocking one coordination site and sterically limiting coordination of the other to water. The use of chloride as the counterion, on the other hand, results in the formation of only one complex (**1**) with a 4 : 1 ligand : metal ratio using pyrazole. The other three complexes (**3**, **5**, and **7**) incorporating methylated pyrazoles form complexes with 2 : 1 ligand : metal ratios, with two of these (**5** and **7**) containing bridging chlorides.

The crystal density follows a clear downward trend as the extent of pyrazole substitution increases (figure 19). Complexes **1** and **2** are comparable in their crystal densities, as expected considering their similar coordination modes and crystal packing. Upon adding a methyl group to pyrazole in the 3(5)-position, the density of the complex with $Cu(NO_3)_2$ (**6**) decreases due to the increased steric bulk of the ligand and its subsequent effect on the crystal packing. This trend continues in both 3,5-dimethylpyrazole complexes of Cu^{II} (**7** and **8**).
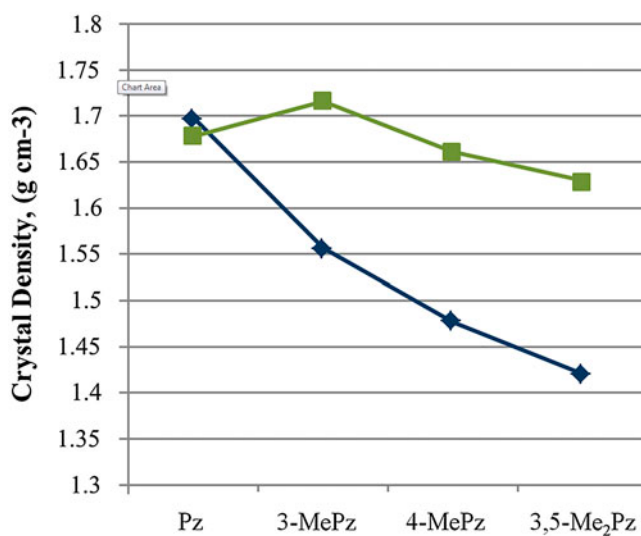
Figure 19. Chart depicting the decrease in coordination complex crystal density (vertical axis) upon increasing extent of methyl substitution for complexes of the ligands (horizontal axis) pyrazole (Pz), 3-methylpyrazole (3-MePz), 4-methylpyrazole (4-MePz), and 3,5-dimethylpyrazole (3,5-Me$_2$Pz) with Cu(NO$_3$)$_2$ (◆) and CuCl$_2$ (■). The lines are guides for the eye.

Upon moving the methyl group to the 4-position, the crystal density decreases further, demonstrating the importance of the substituent position on pyrazole in the packing of their complexes. The methyl group protrudes more from the complex when in the 4-position rather than in the 3(5)-position. This increases the complex's overall width, as measured from one methyl carbon to the corresponding carbon on the opposing ligand, from 10.97 Å in **6** to 11.28 Å in the 4-methylpyrazole complex (**4**), slightly reducing its overall density.

In the case of the complexes with chloride as the counterion, there is actually a slight increase in crystal density from pyrazole to 3-methylpyrazole. This is attributed to the significant change in the structure of the complex from a discrete mononuclear complex (**1**) to a chloride-bridged complex (**5**). After this initial increase, complexes **3**, **5**, and **7** follow the same downward trend in crystal density observed for the corresponding nitrate complexes, although not as pronounced. In general, the complexes containing chloride as the counterion have higher resulting crystal densities as a direct result of forming only 2 : 1 complexes with the methylated pyrazoles, allowing chloride bridging and more efficient packing of the complex in the crystal structure. Complex **3** does not form a bridged species, but otherwise packs in a manner similar to the 3(5)-methylpyrazole congener (**5**).

The crystal density again decreases upon coordinating 3,5-dimethylpyrazole in both the chloride and nitrate cases. In the case of **8**, this decrease is likely due to the expulsion of the nitrate anions from the first coordination sphere as a result of the blocking effect of the methyl groups on the axial coordination sites of Cu^{II} and the subsequent enlargement of the unit cell. For **7**, this change is attributed to both the change in ligand coordination (from *trans* in **3** and **5** to *cis* in **7**) as well as the resulting change in dimer packing from a compact herringbone pattern to a more open packing. Both of these changes are a direct result of the additional steric hindrance introduced by the second methyl group on the pyrazole ligand.

4.2. *Electronic trends*

The pyrazole $\pi \rightarrow Cu^{II}$ d_{xy} LMCT absorption energy decreases upon subsequent methyl sub-stitution in the order pyrazole > 3(5)-methylpyrazole ≈ 4-methylpyrazole > 3,5-dimethylpyrazole. The d_{xy} orbital must be the interacting orbital as it is properly aligned with the pyrazole ligand π-orbitals on account of the pyrazole ligand's perpendicular orien-tation with respect to the axially elongated *z*-axis of the complexes. The lower energy gap between the pyrazole π-orbital and the Cu^{II} d_{xy} orbital indicates a slight destabilization of the π-orbital that is directly correlated to the number of methyl groups residing on the pyra-zole core, regardless of substituent position.

   As Cu^{II} is a d^9 metal ion, the energy of the visible absorption is directly related to the ligand-field splitting energy and can be easily calculated from the wavelength of absorption (figure 20). The overall decrease in the d–d transition energy from the nitrate complexes (**4**, **6**, and **8**) to the chloride complexes (**3**, **5**, and **7**) of methyl-substituted pyrazole is explained by the replacement of two pyrazole ligands in the former for the weaker field chloride ligand in the latter. Solvent-induced changes in the visible absorption wavelength for the Cl^- complexes indicate exchange of the Cl^- ligands with water in solution, as shown by the higher d–d transition energy in water relative to methanol, demonstrating the expected destabilization of the d_{x2-y2} orbital by water upon displacement of the Cl^- ligands present in the solid state. The nitrate complexes, however, undergo no similar solvent-based variation, indicating that the pyrazole ligands are not displaced in either solvent, as this variation in the d–d transition in the chloride complexes is due to the displacement of the
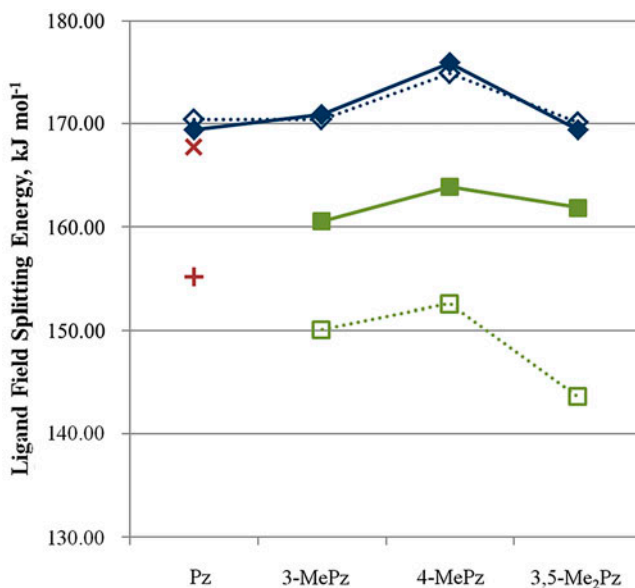

Figure 20. Chart depicting the modulation of ligand-field splitting energy in kJ mol^{-1} (vertical axis, as calculated from λ_{max} of the visible absorption band) for the complexes of the ligands (horizontal axis) pyrazole (Pz), 3-methylpyrazole (3-MePz), 4-methylpyrazole (4-MePz), and 3,5-dimethylpyrazole (3,5-Me$_2$Pz) with Cu(NO$_3$)$_2$ (◆,◇) and CuCl$_2$ (■,□) in water (solid) and methanol (open). The pyrazole complexes of CuCl$_2$ (✕, water; +, methanol) are separated from the other CuCl$_2$ complexes on account of their different ligand to metal ratio (4 : 1 *vs.* 2 : 1). Lines (solid, water; dotted, methanol) are provided as guides for the eye.

chloride anions in the equatorial square plane, directly affecting the energy of the d_{x2-y2} orbital, in water but not in methanol, whereas the nitrate complexes have four pyrazole ligands in the equatorial plane, leaving the d_{x2-y2} orbital unperturbed in either solvent. Considering both the similarity in ligand-field splitting energy between **1** and **2** in water and the displacement of chloride by water in the complexes of the methylated pyrazoles, it is inferred that the nitrate ligands are removed from the coordination sphere of the complexes, but not necessarily replaced by coordinated water.

Most interesting, however, is the modulation of the d–d transition energy in the visible region resulting from methyl substitution on pyrazole. Surprisingly, the greatest effect on the energy of the d–d transition is not from the extent of substitution, but the position of substitution on the pyrazole core. For all complexes in both methanol and water, coordination of 4-methylpyrazole leads to the highest energy visible absorption, including 3,5-dimethylpyrazole. This shows the significant effect electron-donating substituents at the 4-position have on the electron density at the coordinating N2 position of pyrazole, as the increased electron density at this location leads to a destabilization of the Cu^{II} d_{x2-y2} orbital from σ-type interactions with the ligand. This effect may be a contributing factor to the lack of chloride bridging in **3**.

5. Conclusions

Changes in the counterion and methyl substitution on pyrazole significantly affect the coordination environment, crystal density, and electronic properties of the resulting complexes with Cu^{II}, despite strict control of the reaction conditions. Crystal structures of the copper (II) chloride and nitrate complexes with 3(5)- and 4-methylpyrazole have been determined for the first time, while those of pyrazole and 3,5-dimethylpyrazole have been reproduced. In addition, a systematic study of the electronic absorption properties of all complexes in both water and methanol has revealed a surprising trend in the d–d transition of Cu^{II} as a function of substituent position on pyrazole.

With chloride as the counterion, the complexes of all methylated pyrazoles form with 2 : 1 ligand : metal ratios and higher density; the pyrazole complex forms a 4 : 1 complex similar in both coordination and density to that with copper(II) nitrate. In all chloride complexes, the ion remains in the inner coordination sphere, though subject to varying degrees of Jahn–Teller distortion. The nitrate complexes form with 4 : 1 metal:ligand ratios and, save the 3,5-dimethylpyrazole congener (**8**), coordinated nitrate. All complexes pack without interstitial solvent molecules. In general, higher crystal densities occur with decreasing methyl substitution, in the order pyrazole > 3(5)-pyrazole > 4-methlypyrazole > 3,5-dimethylpyrazole. Though the extent of methyl substitution affected the pz $\pi \rightarrow$ Cu^{II} d_{xy} LMCT band (more methyl groups, lower energy transition), the position of the methyl group on the pyrazole core was found to be the critical factor in modulating the Cu^{II} d–d transition, with the 4-methylpyrazole complexes exhibiting the highest d–d transition energy of all complexes analyzed.

The results presented herein demonstrate that the extent and position of methyl substitution on pyrazole and the choice of counterion are the primary factors in determining the ligand to metal ratio and final structure of the complex, as well as modulating the electronic absorption properties. The effects observed thus far by these small perturbations suggest that complex formation would be sensitive to other factors, such as reaction solvent

coordination strength, and could play a role in tuning-specific structural and electronic properties in complexes of other pyrazole ligands.

Acknowledgements

Disclosure statement

No potential conflict of interest was reported by the authors.

Funding

Supplemental data

Crystallographic parameters are listed for **1, 2, 7,** and **8**. Full tables of bond lengths and angles are provided for all complexes presented. CCDC 1056648–1056654, 1056667 contain the supplementary crystallographic data for this article. These data can be obtained free of charge from The Cambridge Crystallographic Data Center via www. ccdc.cam.ac.uk/data_request/cif. Comparison charts of UV-vis spectra are also included. Supplemental data for this article can be accessed here [http://dx.doi.org/10.1080/00958972.2015.1077952].

ORCID

Ian D. Giles 🅳 http://orcid.org/0000-0002-9421-5365
Jeffrey R. Deschamps 🅳 http://orcid.org/0000-0001-5845-0010

References

[1] (a) M. Inoue, M. Kishita, M. Kubo. *Inorg. Chem.*, **4**, 626–628 (1965); (b) M.H. Mihailov, V.T. Mihailova, V.A. Khalkin. *J. Inorg. Nucl. Chem.*, **36**, 141–144 (1974); (c) D. Nicholls, B.A. Warburton. *J. Inorg. Nucl. Chem.*, **33**, 1041–1045 (1971); (d) J. Reedijk. *Recl. Trav. Chim. Pays-Bas*, **89**, 605–619 (1970); (e) J. Reedijk. *Recl. Trav. Chim. Pays-Bas*, **89**, 993–1016 (1970); (f) J. Reedijk. *Recl. Trav. Chim. Pays-Bas*, **90**, 117–129 (1971); (g) J. Reedijk, J.A. Smith. *Recl. Trav. Chim. Pays-Bas*, **90**, 1135 (1971); (h) J. Reedijk, J.C.A. Windhorst, N.H.M. Van Ham, W.L. Groeneveld. *Recl. Trav. Chim. Pays-Bas*, **90**, 234–251 (1971); (i) C.B. Singh, S. Satpathy, B. Sahoo. *J. Inorg. Nucl. Chem.*, **35**, 3947–3950 (1973); (j) R.W.M. Tenhoedt, F.B. Hulsbergen, G.C. Verschoor, J. Reedijk. *Inorg. Chem.*, **21**, 2369–2373 (1982).
[2] (a) A. Mighell, A. Santoro, E. Prince, C. Reimann. *Acta Crystallogr., Sect. B: Struct. Sci.*, **31**, 2479–2482 (1975); (b) K. Sakai, Y. Yamada, T. Tsubomura, M. Yabuki, M. Yamaguchi. *Inorg. Chem.*, **35**, 542–544 (1996).
[3] (a) V. Chandrasekhar, S. Kingsley, A. Vij, K.C. Lam, A.L. Rheingold. *Inorg. Chem.*, **39**, 3238–3242 (2000); (b) N.V. Pervukhina, N.V. Podberezskaya, L.G. Lavrenova. *J. Struct. Chem.*, **36**, 138–145 (1995).
[4] Bruker. *APEX2 (v2013.10-0),* Bruker AXS Inc., Madison, WI (2013).
[5] Bruker. *SAINT (v8.34a),* Bruker AXS Inc., Madison, WI (2013).
[6] Bruker. *XPREP (v2013/3),* Bruker AXS Inc., Madison, WI (2013).
[7] Bruker. *SADABS (v2012/1),* Bruker AXS Inc., Madison, WI (2012).

[8] (a) Bruker. *SHELXTL (v2013/4),* Bruker AXS Inc., Madison, WI (2013); (b) G. Sheldrick. *Acta Crystallogr., Sect. A: Found. Crystallogr.*, **64**, 112–122 (2008).

[9] L.J. Barbour. *J. Supramolecular Chemistry*, **1**, 189–191 (2001).

[10] (a) U. Casellato, R. Ettorre, R. Graziani. *Z. Krist.-New Cryst. St.*, **215**, 287–288 (2000); (b) Y.J. Sun, P. Cheng, S.P. Yan, D.Z. Liao, Z.H. Jiang, P.W. Shen. *J. Mol. Struct.*, **597**, 191–198 (2001); (c) Y.H. Xing, J. Han, B.L. Zhang, X.J. Zhang, Y.H. Zhang, G.H. Zhou. *Acta Crystallogr. Sect. E: Struct. Rep. Online*, **62**, M3354–M3356 (2006).

[11] (a) A.M. Mills, K. Flinzner, A.F. Stassen, J.G. Haasnoot, A.L. Spek. CCDC 179047: Private communication to the Cambridge Structural Database (2002); (b) E. Mutsenek, M. Bolte. CCDC 821652: Private communication to the Cambridge Structural Database (2011).

[12] J.L. Shaw, T.B. Cardon, G.A. Lorigan, C.J. Ziegler. *Eur. J. Inorg. Chem.*, **2004**, 1073–1080 (2004).

[13] B. Barszcz, T. Głowiak, J. Jezierska, A. Tomkiewicz. *Polyhedron*, **23**, 1309–1316 (2004).

[14] G.A. van Albada, M.G. van der Horst, I. Mutikainen, U. Turpeinen, J. Reedijk. *Inorg. Chim. Acta*, **361**, 3380–3387 (2008).

[15] E. Bernarducci, W.F. Schwindinger, J.L. Hughey, K. Krogh-Jespersen, H.J. Schugar. *J. Am. Chem. Soc.*, **103**, 1686–1691 (1981).

[16] D.S. Noyce, E. Ryder, B.H. Walker. *J. Org. Chem.*, **20**, 1681–1686 (1955).